Effects of shape and dopant on structural, optical absorption, Raman, and vibrational properties of silver and copper quantum clusters: A density functional theory study*

Li Wei-Yin(李维银) and Chen Fu-Yi(陈福义)†

State Key Laboratory of Solidification Processing, Northwestern Polytechnical University, Xi'an 710072, *China*

(Received 16 April 2014; revised manuscript received 26 May 2014; published online 10 September 2014)

We investigate the effects of shape and single-atom doping on the structural, optical absorption, Raman, and vibrational properties of Ag_{13}, $Ag_{12}Cu_1$, Cu_{13}, and $Cu_{12}Ag_1$ clusters by using the (time-dependent) density functional theory. The results show that the most stable structures are cuboctahedron (COh) for Ag_{13} and icosahedron (Ih) for Cu_{13}, $Ag_{12}Cu_{1core}$, and $Cu_{12}Ag_{1sur}$. In the visible–near infrared optical absorption, the transitions consist of the interband and the intraband transitions. Moreover, red shifts are observed as follows: 1) clusters change from $Ag_{12}Cu_{1core}$ to Ag_{13} to $Ag_{12}Cu_{1sur}$ with the same motifs, 2) the shapes of pure Ag_{13} and $Ag_{12}Cu_{1core}$ clusters change from COh to Ih to decahedron (Dh), 3) the shape of $Ag_{12}Cu_{1sur}$ clusters changes from Ih to COh to Dh, and 4) the shapes of pure Cu_{13} and $Cu_{12}Ag_1$ clusters change from Ih to Dh to COh. All of the Raman and vibrational spectra exhibit many significant vibrational modes related to the shapes and the compositions of the clusters. The ranges of vibrational spectra of Ag_{13}, $Ag_{12}Cu_1$ or Cu_{13}, and $Cu_{12}Ag_1$ clusters become narrower and the vibrational intensities increase as the shape of the clusters changes from Ih to Dh to COh.

Keywords: stability, optical absorption, Raman spectroscopy, nanoclusters

PACS: 71.45.Gm, 42.25.Bs, 72.15.Nj, 73.20.Mf **DOI:** 10.1088/1674-1056/23/11/117103

1. Introduction

Metal clusters smaller than 2 nm in diameter have discrete electronic levels due to the quantum size effects.[1,2] Hence, they show optical absorption in the visible and the near infrared regions, and exhibit various properties, such as fluorescence,[3,4] two-photon absorption,[5] and paramagnetism,[6] which are different from those of bulk metal and metal nanoparticles larger than 3 nm in diameter. For example, recently, a new class of noble metal-cluster sensitizer was explored use in high-efficiency solar cells.[7,8]

Bimetallic nanoclusters have recently received considerable interest for their particular and unique structural, electronic,[9,10] optical,[11,12] and magnetic properties, as well as their importance in catalysis.[13] It is found that their physical and chemical properties depend on the size, structure, and chemical ordering of their components.[14–19] Scholl,[20] Lee *et al.*,[21] Noguez,[22] Dong *et al.*,[23] Gong *et al.*,[24] and Guidez *et al.*[25] revealed that the optical properties of metal clusters depend on their sizes, shapes, metal compositions, and surrounding environments. Baishya *et al.*[26] indicated that more than one isomer of Ag clusters can contribute to the measured spectrum at specific sizes. Durante *et al.*[27] showed that the center of the absorption peak weakly depends on the cluster shape, whereas the maximum of the absorption peak strongly depends on the cluster shape. Weissker *et al.*[28] found that the atomic-level structural details are important in explaining the size range differences appearing in the lower part of the spectrum of smaller clusters. Bae *et al.*[29] predicted that the absorption peak maximum red shifts as the cluster enlarges and blue shifts as the shape of the cluster changes from octahedron to icosahedron (Ih). In our previous investigations, we calculated the structural and optical properties of 7-, 8-, 13-, and 55-atom Ag–Cu[30–36] and the transition-metal-doped Ag chains.[37]

According to Weissker's reports,[28] as the size becomes smaller, the number of possible symmetries becomes larger. In the present work, we concentrate on high-symmetry structures with magic size (compact atomic shells) for 13-atom pure clusters[38,39] and single-atom dopant clusters: icosahedron (Ih), cuboctahedron (COh), and decahedron (Dh) (illustrated in Fig. 1). These structural motives of the pure clusters have all been found experimentally, albeit for somewhat larger clusters.[40–42] These clusters are all approximately spherical, which allows us to study the influence of the structural differences on the spectra without strong morphological effects. However, unlike some of the structures treated in the previous studies,[43–45] they are not necessarily the lowest-energy structures. In the case of the 13-atom clusters, there is a large number of possible symmetries, and the lowest ones are neither icosahedral nor cubic.[46–52]

*Project supported by the National Natural Science Foundation of China (Grant Nos. 51271148 and 50971100), the Research Fund of State Key Laboratory of Solidification Processing in China (Grant No. 30-TP-2009), the Aeronautic Science Foundation Program of China (Grant No. 2012ZF53073), and the Doctoral Fund of the Ministry of Education of China (Grant No. 20136102110013).

†Corresponding author. E-mail: fuyichen@nwpu.edu.cn

© 2014 Chinese Physical Society and IOP Publishing Ltd

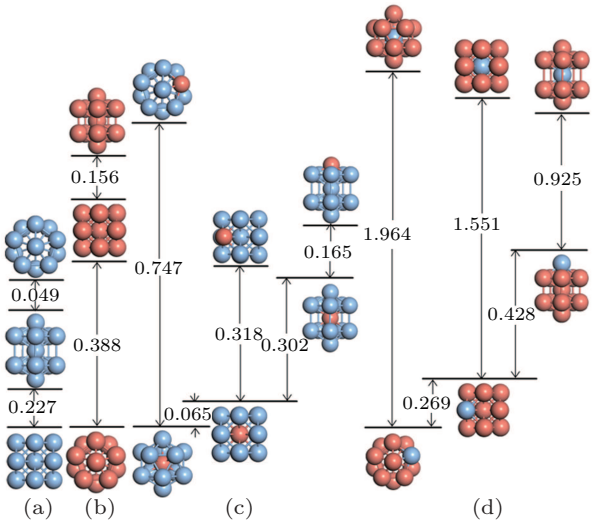


Fig. 1. (color online) Energy differences between isomer structures of (a) pure Ag_{13}, (b) Cu_{13}, (c) $Ag_{12}Cu_1$, and (d) Ag_1Cu_{12} clusters with three types of structures, namely, Ih, COh, and Dh, after optimization. All energies are in units of eV.

In this study, we investigate the effects of shapes and dopant on the structural, optical absorption, vibrational, and Raman properties of 13-atom pure Ag and Cu, and Ag–Cu clusters. We also examine in detail the electron excitation process in the visible–near infrared (Vis–NIR) optical absorption.

2. Models and computational method

In this paper, we prepare pure Ag_{13}, Cu_{13}, $Ag_{12}Cu_1$, and $Cu_{12}Ag_1$ with three types of structures, namely, Ih, COh, and Dh, for effective analysis. These structures are well known as cluster isomers with 13 atoms, especially the former two structures. The prepared structures are optimized using density functional theory (DFT) calculations carried out on selected configurations using the $Dmol^3$ package that is included in materials studio.[53,54] Spin-polarized DFT calculations are performed in real space within the framework of DFT-based semi-core pseudopotentials (DSPPs)[55] with the double numerical plus polarization (DNP) function. A global cutoff of 5.0 Å is used for grid integration. Self-consistent field procedures are performed with a convergence criterion of 10^{-6} Hartree on the total energy and the electron density. The Perdew *et al.*[56] generalized gradient approximation (PBE/GGA) is used for the exchange–correlation functional during the geometry optimization for the Ag cluster.[30–33,37,43,57] The boundary condition of all of the clusters is in vacuum.

The binding energies, Mulliken atomic charges, Raman spectra, and vibrational spectra are also obtained under the PBE/GGA. The Raman spectra of the clusters are simulated with an incident light of 514.5 nm at 10 K. The absorption property calculations of the clusters are performed under the PBE/GGA using TD-DFT.[58]

The PBE potential and the DSPP/DNP basis set are used to calculate the lowest excited states of the Ag dimer, and the results show that the lowest excited state is 3.11 eV at an oscillator intensity of $f = 0.36$ a.u. These values well agree with the experimental value of 3.20 eV[59,60] and earlier TDLDA results of 3.20 eV at $f = 0.32$ a.u.,[61,62] 3.11 eV at $f = 0.33$ a.u.,[63] and 3.2 eV.[64,65] Therefore, the selected potential and basis set are reasonably well used to calculate the lowest excited states of the Ag clusters.

3. Results and discussion

Figure 1 shows the Ag_{13}, Cu_{13}, $Ag_{12}Cu_1$, and Ag_1Cu_{12} clusters of structures Ih, COh, and Dh after the optimization using DFT. All of the clusters after the optimization show the same structures and symmetry point groups as before the optimization (Table 1). In a pure Ag_{13} cluster, the total energy of COh with O_h point group symmetry exceeds that of Dh with D_{5h} point group symmetry by 0.227 eV, and the later exceeds that of Ih with I_h point group symmetry by 0.049 eV. These results indicate that the order of stability is COh, Dh, and Ih. This result well agrees with some previous results,[28,66] showing that COh is more stable than Ih, but differs from other reports.[67–74] For the Cu_{13} cluster, the total energy of Ih with I_h point group symmetry exceeds that of COh with O_h point group symmetry by 0.388 eV, and the latter exceeds that of Dh with D_{5h} point group symmetry by 0.156 eV. These results indicate that the decreasing order of stability is Ih, COh, and Dh, which is in agreement with Shin's report[66] but differs from the other reports.[28,67,68,70,72,73,75–77] The energy difference between COh and Ih in pure Ag cluster is smaller than the corresponding energy difference in a pure Cu cluster, which is opposite to Shin's report.[66]

Table 1. Symmetry point group (PG), binding energy (E_b), total Mulliken positive charge (TPC), and total bond number (TBN) of the clusters.

Cluster	PG	E_b/eV	TPC	TBN
Ih Ag_{13}	I_h	–18.68206	0.209	42
Dh Ag_{13}	D_{5h}	–18.73153	0.249	37
COh Ag_{13}	O_h	–18.95847	0.241	36
Ih Cu_{13}	I_h	–27.81903	0.208	42
Dh Cu_{13}	D_{5h}	–27.27508	0.203	37
COh Cu_{13}	O_h	–27.43099	0.219	36
Ih $Ag_{12}Cu_{1core}$	I_h	–19.93397	0.251	42
Ih $Ag_{12}Cu_{1sur}$	C_{5v}	–19.18727	0.237	42
Dh $Ag_{12}Cu_{1core}$	D_{5h}	–19.56710	0.264	37
Dh $Ag_{12}Cu_{1sur}$	C_{5v}	–19.40207	0.231	37
COh $Ag_{12}Cu_{1core}$	O_h	–19.86921	0.232	36
COh $Ag_{12}Cu_{1sur}$	C_{2v}	–19.55135	0.203	36
Ih $Cu_{12}Ag_{1core}$	I_h	–25.15486	0.206	42
Ih $Cu_{12}Ag_{1sur}$	C_{5v}	–27.11900	0.205	42
Dh $Cu_{12}Ag_{1core}$	D_{5h}	–25.49671	0.218	37
Dh $Cu_{12}Ag_{1sur}$	C_{5v}	–26.42201	0.198	37
COh $Cu_{12}Ag_{1core}$	O_h	–25.29934	0.338	36
COh $Cu_{12}Ag_{1sur}$	C_{2v}	–26.84988	0.220	36

The Cu atom-doped Ag_{13} cluster (i.e., $Ag_{12}Cu_1$) includes two configurations: $Ag_{12}Cu_{1core}$ (Cu atom doping in the core

of pure Ag_{13} cluster) and $Ag_{12}Cu_{1sur}$ (Cu atom doping on the surface of pure Ag_{13} cluster) (Fig. 1(c)). The $Ag_{12}Cu_{1core}$ cluster with any configuration (Ih, COh, or Dh) is more stable than the $Ag_{12}Cu_{1sur}$ cluster with the same configuration, which is in agreement with Shin's report[66] for Ih and COh and Bochicchio's report for Ih.[78] The stability of the $Ag_{12}Cu_{1core}$ cluster with Ih shape exceeds that with COh shape by 0.065 eV, different from Shin's results that the $Ag_{12}Cu_{1core}$ cluster with a COh shape which exceeds that with Ih shape by 0.169 eV.[66] The stability of the $Ag_{12}Cu_{1core}$ cluster with COh shape exceeds that with Dh shape by 0.302 eV.

In the case of the Ag-atom doped Cu_{13} cluster (i.e., $Cu_{12}Ag_1$), two configurations exist: $Cu_{12}Ag_{1core}$ (Ag atom doped in the core of pure Cu_{13} cluster) and $Cu_{12}Ag_{1sur}$ (Ag atom doped on the surface of pure Cu_{13} cluster) (Fig. 1(d)). In any configuration (Ih, COh, or Dh), the $Cu_{12}Ag_{1sur}$ cluster is more stable than the $Cu_{12}Ag_{1core}$ cluster, which is in agreement with Bochicchio's report for Ih.[78] The $Cu_{12}Ag_{1sur}$ cluster with Ih shape is more stable than that with COh shape by 0.269 eV, and the latter is more stable than that with Dh shape by 0.428 eV.

The surface energy of Ag (78 meV/Å^2) is less than that of Cu (113.9 meV/Å^2),[79] which favors surface enrichment by Ag and core enrichment by Cu; thus, the surface energy forces the formation of high-stability $Ag_{12}Cu_{1core}$ and $Cu_{12}Ag_{1sur}$ clusters. For the case of the $Ag_{12}Cu_1$ cluster, the preferential inner placement of Cu impurities in the Ih 13-atom cluster is due mainly to the very effective strain relaxation, as previously reported,[80,81] which is achieved by putting a smaller Cu atom in the compressed center of the icosahedral cluster. As shown in Table 2, the coordination number of 12 for the core-doped Cu atom is larger than that of 5 or 6 for the surface-doped Cu atom. Moreover, the Mulliken positive charges of 0.251 for Ih, 0.264 for Dh, and 0.232 for COh for the core-doped Cu atom are larger than those of 0.237 for Ih, 0.231 for Dh, and 0.203 for COh for the surface-doped Cu atom. Therefore, forming stable $Ag_{12}Cu_{1core}$ clusters is related to the surface energy, maximizing the number of Ag–Cu bonds, the charge transfer, and the strain relaxation. In the case of the $Cu_{12}Ag_1$ cluster, the number of Cu–Cu bonds of the $Cu_{12}Ag_{1sur}$ cluster is larger than that of the $Cu_{12}Ag_{1core}$ cluster (Table 2) with the same configuration, so the stability of the $Cu_{12}Ag_1$ cluster is related to the total bond number of Cu–Cu bonds. Overall, the stability of the Ag–Cu nanoclusters depends on the strain relaxation, the bond number, the surface energy, and the charge transfer.

The ultraviolet (UV), visible (Vis), and near infrared (NIR) optical absorption spectra of neutral pure Ag_{13}, pure Cu_{13}, $Ag_{12}Cu_1$, and $Cu_{12}Ag_1$ clusters with Ih, Dh, and COh motifs are shown in Fig. 2 and Table 2 for UV–Vis and Fig. 3 for Vis–NIR as calculated by the improved TD-DFT. The UV–Vis optical absorption spectra are compared in Fig. 2 and the corresponding absorption peaks are listed in Table 2 in the form of position energy (eV) and intensity (arb. units). The experimental position energies of the Ag_{13} cluster lie at 3.38 eV with maximum intensity, 3.83 eV with minimum intensity, 4.42 eV with secondary intensity in Ref. [60], and 3.40 eV with maximum intensity, 3.90 eV with secondary intensity, and 4.40 eV with minimum intensity in Ref. [44].

Table 2. Position energies (in units of eV) and intensities (in arb. units) of the calculated absorption peaks in UV–Vis spectra for the clusters.

Cluster	Ih	Dh	COh
Ag_{13}	2.17 (0.024)	2.00 (0.020)	2.43 (0.063)
	2.69 (0.065)	2.23 (0.012)	2.72 (0.022)
	2.95 (0.049)	2.35 (0.017)	2.92 (0.045)
	3.41 (0.240)	2.72 (0.025)	3.29 (0.276)
	3.84 (1.733)	3.81 (2.078)	3.68 (1.106)
	4.37 (0.951)	4.38 (0.822)	4.00 (1.327)
			4.48 (0.917)
Cu_{13}	2.73 (0.081)	2.19 (0.014)	1.92 (0.011)
	3.41 (0.782)	2.74 (0.066)	2.28 (0.027)
		3.16 (0.454)	3.20 (0.512)
		3.39 (0.530)	
$Ag_{12}Cu_{1core}$	2.24 (0.013)	2.18 (0.013)	2.47 (0.036)
	2.64 (0.102)	2.43 (0.011)	2.71 (0.026)
	3.35 (0.209)	2.63 (0.019)	3.26 (0.424)
	3.83 (1.800)	3.12 (0.101)	3.66 (0.989)
	4.40 (0.616)	3.72 (1.539)	3.90 (0.958)
		4.31 (0.454)	4.51 (0.812)
$Ag_{12}Cu_{1sur}$	2.25 (0.070)	2.34 (0.038)	2.49 (0.036)
	2.67 (0.064)	2.43 (0.034)	2.84 (0.054)
	3.13 (0.103)	2.76 (0.018)	3.03 (0.079)
	3.80 (1.246)	2.94 (0.030)	3.71 (0.977)
		3.78 (1.515)	3.95 (1.087)
		4.29 (0.906)	4.40 (0.832)
$Cu_{12}Ag_{1core}$	2.46 (0.025)	2.23 (0.040)	2.33 (0.101)
	2.71 (0.040)	3.00 (0.251)	2.62 (0.121)
	3.23 (0.627)	3.25 (0.126)	2.82 (0.019)
	3.46 (0.478)		3.16 (0.531)
$Cu_{12}Ag_{1sur}$	2.70 (0.117)	2.22 (0.013)	2.30 (0.017)
	3.51 (0.583)	2.76 (0.046)	2.67 (0.020)
		3.20 (0.599)	2.86 (0.032)
			3.22 (0.389)

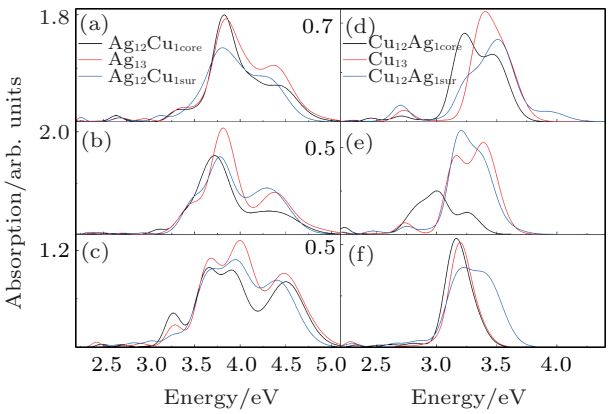


Fig. 2. (color online) UV–Vis optical absorption spectra for pure Ag_{13} and $Ag_{12}Cu_1$ (left) with Ih (a), Dh (b), and COh (c) motifs, and pure Cu_{13} and $Cu_{12}Ag_1$ (right) clusters with Ih (d), Dh (e), and COh (f) motifs calculated by the improved TD-DFT. The smearing band is 20.0 nm.

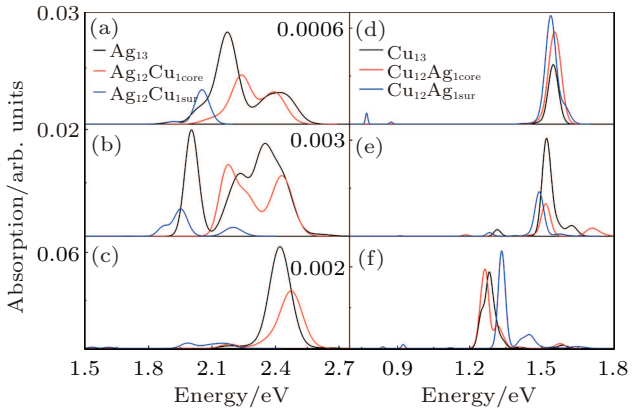


Fig. 3. (color online) Vis–NIR optical absorption spectra for pure Ag_{13} and $Ag_{12}Cu_1$ (left) with Ih (a), Dh (b), and COh (c) motifs, and pure Cu_{13} and $Cu_{12}Ag_1$ (right) clusters with Ih (d), Dh (e), and COh (f) motifs calculated by the improved TD-DFT. The smearing band is 20.0 nm.

The theoretical optical absorption spectra of pure Ag_{13} clusters are shown in Figs. 2(a)–2(c) and Table 2. The strongest peaks of Ih, Dh and COh Ag_{13} lie at 3.84 eV, 3.81 eV, and 4.00 eV, respectively. These peak positions in the theoretical spectra are in excellent agreement with both the reported experimental results and the previously calculated values.[26,28,75,82] The calculated UV–Vis optical absorption spectra of pure Cu_{13} clusters are displayed in Figs. 2(d)–2(f) and Table 2. The main peaks of Ih, Dh and COh Cu_{13} lie at 3.41 eV, 3.39 eV, and 3.20 eV, respectively. The peak positions in the spectra are close to those previously obtained by Baishya.[75]

The UV–Vis optical absorption spectrum of the Ih $Ag_{12}Cu_{1core}$ cluster has five absorption peaks, while the UV–Vis spectra of the Dh and COh motifs have six absorption peaks (Figs. 2(a)–2(c) and Table 2). The position energies and intensities of the maximum peaks obey the order Ih > Dh > COh. Compared with that of pure Ag_{13} clusters, the maximum peak of the Ih $Ag_{12}Cu_{1core}$ cluster lowers in the position energy by 0.01 eV but its intensity strengthens; both position energies and intensities of the maximum peaks of Dh and COh $Ag_{12}Cu_{1core}$ clusters are lower. Compared with those of pure Cu_{13} clusters, position energies and intensities of the maximum peaks of Ih, Dh, and COh $Ag_{12}Cu_{1core}$ clusters increase.

For the UV–Vis spectra of the $Ag_{12}Cu_{1sur}$ clusters, there are four absorption peaks in Ih, six peaks in Dh and COh motifs (Figs. 2(a)–2(c) and Table 2). The position energies of the maximum peaks obey the order COh > Ih > Dh. The intensities of the maximum peaks obey another order Dh > Ih > COh. For the excited energies and the intensities of the maximum peaks, Ih, Dh and COh $Ag_{12}Cu_{1sur}$ clusters are lower when compared with pure Ag_{13} clusters, while Ih, Dh and COh $Ag_{12}Cu_{1sur}$ clusters increase as compared with pure Cu_{13} clusters.

Ih and COh $Cu_{12}Ag_{1core}$ clusters have four absorption peaks in the UV–Vis spectra, while the Dh motif has three peaks (Figs. 2(d)–2(f) and Table 2). The main peak of Ih is the strongest of all, and the peak of Dh is the weakest of all. For the excited energies and the intensities of the maximum peaks, Ih and Dh $Cu_{12}Ag_{1core}$ clusters are lower when compared with pure Ag_{13} and Cu_{13} clusters. The maximum peak of COh lowers in the position energy but strengthens in the intensity compared with that of pure Ag_{13} and Cu_{13} clusters.

For the UV–Vis optical absorption spectra of $Cu_{12}Ag_{1sur}$ clusters (Figs. 2(d)–2(f) and Table 2), Ih has two peaks, Dh has three peaks, and COh has four peaks. The main peak of Dh is the strongest of all, and the peak of COh is the weakest of all. For the excited energies and the intensities of the maximum peaks, Ih, Dh and COh clusters are lower when compared with pure Ag_{13}. Compared with those of Cu_{13} clusters, the maximum peaks of Ih and COh increase in position energy but weaken in intensity; the maximum peak of Dh lowers in position energy but strengthens in intensity.

To limit the studies of the optical absorption spectra of pure Ag_{13}, Cu_{13}, $Ag_{12}Cu_1$, and $Cu_{12}Ag_1$ neutral clusters in the Vis–NIR wavelength range, we further investigate and compare their Vis–NIR optical absorption extinction spectra in Fig. 3. The electronic energy levels, density of state (DOS), and contributions of s, p, and d electrons for pure Ag_{13} cluster with COh calculated by GGA/DFT are shown in Fig. 4. The COh Ag_{13} cluster in the Vis–NIR has only one strong peak, which lies at 2.42 eV ($f = 0.0636$ a.u.) (Fig. 3(c)) and can be assigned to a combination of HOMO-1, HOMO-4 → LUMO+11, LUMO+12, HOMO-2, and HOMO-5 → LUMO+12. The primary transitions are sd → spd (Fig. 4). The results in Fig. 4 can be attributed to the up and down spin electrons in the same decadency, and the contributions of s, p, and d electrons that are less than 10% are neglected. Thus, only one type of transition exists: the interband transition from HOMO to LUMO in the COh Ag_{13} cluster. Correspondingly, the COh $Ag_{12}Cu_{1core}$ cluster has two strong peaks in the Vis–NIR (Fig. 3(c)). The stronger peak located at 2.47 eV arises from the interband transitions, and the primary transitions are spd → spd. The other peak located at 2.18 eV arises from the intraband transitions, which are from HOMO to HOMO transitions. The primary transitions are also spd → spd. The COh $Ag_{12}Cu_{1sur}$ cluster also has two peaks in the Vis–NIR, which arise from the interband transitions, and the primary transitions are d → spd.

Ag_{13} and $Ag_{12}Cu_{1core}$ clusters with Ih motif have two peaks, while the Ih $Ag_{12}Cu_{1sur}$ cluster has only one peak in the Vis–NIR (Fig. 3(a)). The peaks of these three clusters in the Vis–NIR arise from different interband transitions: the primary transitions for Ag_{13} and $Ag_{12}Cu_{1core}$ clusters are spd → d, while the primary transitions for the $Ag_{12}Cu_{1sur}$ cluster are pd → d.

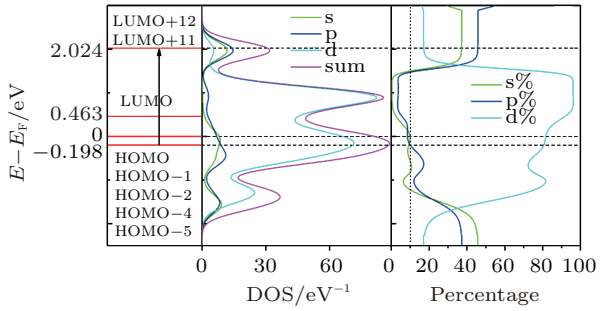


Fig. 4. (color online) Electronic energy levels (left), DOS (middle), and contribution of s, p, and d electrons (right) for pure Ag_{13} cluster with COh calculated by GGA/DFT. The smearing width is 0.0073499 Hartree.

The Dh Ag_{13} cluster has three strong peaks, while Dh $Ag_{12}Cu_{1core}$ and Dh $Ag_{12}Cu_{1sur}$ clusters have two strong peaks in the Vis–NIR (Fig. 3(b)). Their absorption peaks in the Vis–NIR arise from the interband transitions: the primary transitions for Ag_{13} and $Ag_{12}Cu_{1core}$ clusters are d → spd, and the primary transitions for the $Ag_{12}Cu_{1sur}$ cluster are spd → d and spd → spd.

In the Vis–NIR, the Ih Cu_{13} cluster has only one peak (Fig. 3(d)), which can be assigned to the interband transitions, and the primary transitions are spd → spd. Ih $Cu_{12}Ag_{1core}$ and $Cu_{12}Ag_{1sur}$ clusters have only one peak (Fig. 3(d)), which arises from the interband transitions, and the primary transitions are pd → spd.

In the Vis–NIR, the Dh Cu_{13} cluster has two peaks (Fig. 3(e)). The peak at 1.52 eV can be assigned to the intraband transitions, and the primary transitions are spd → spd. The other peak located at 1.62 eV can be assigned to the interband transitions, and the primary transitions are also spd → spd. The Dh $Cu_{12}Ag_{1core}$ cluster also has two peaks (Fig. 3(e)). The peak at 1.52 eV arises from the intraband transitions, and the primary transitions are spd → spd. The other peak at 1.71 eV arises from the intraband and the interband transitions, and the primary transitions are spd → spd. The Dh $Cu_{12}Ag_{1sur}$ cluster has only one peak (Fig. 3(e)), which arises from the interband transitions, and the primary transitions are spd → spd.

In the Vis–NIR, the COh Cu_{13} cluster has only one peak, while COh $Cu_{12}Ag_{1core}$ and $Cu_{12}Ag_{1sur}$ clusters have two peaks (Fig. 3(f)). All of the transitions arise from the intraband transitions. The primary transitions for the COh Cu_{13} cluster are sp → spd, those for the COh $Cu_{12}Ag_{1core}$ cluster are pd → spd and spd → spd, and those for the COh $Cu_{12}Ag_{1sur}$ cluster are spd → spd.

Therefore, for the optical absorption spectra of Cu_{13} and $Cu_{12}Ag_1$ clusters with Ih, Dh, and COh motifs, the results show that red shifts are presented as the shapes of pure Cu_{13} and $Cu_{12}Ag_1$ clusters change from Ih to Dh and to COh. This phenomenon differs from the tendency of the Ag_{13} cluster. Ag single atom-doped Cu clusters nearly have no effect on the locations of the maximum peaks but result in decreased intensities of optical absorption peaks of Cu_{13} and $Ag_{12}Cu_{1sur}$ clusters with Dh motif and increased intensities of optical absorption peaks of Cu_{13} and $Cu_{12}Ag_{1sur}$ clusters with Ih and Dh motifs. The intensities of optical absorption peaks of $Cu_{12}Ag_{1core}$ clusters are larger than those of $Cu_{12}Ag_{1sur}$ clusters. The peaks of Cu_{13} and $Cu_{12}Ag_1$ clusters with Ih arise from the interband transitions, and the primary transitions for the $Ag_{12}Cu_1$ cluster differ from those for the Ag_{13} cluster. Cu_{13} and $Cu_{12}Ag_{1core}$ clusters with Dh arise from the interband and the intraband transitions, whereas the peaks of the $Cu_{12}Ag_{1sur}$ cluster with Dh arise from the interband transitions. The primary transitions for all clusters with Dh are uniform (spd → spd). All of the peaks of Cu_{13} and $Cu_{12}Ag_1$ clusters with COh arise from the intraband transitions, and the primary transitions for the $Ag_{12}Cu_1$ cluster differ from those for the Ag_{13} cluster.

Figure 5 compares the Raman spectra of pure Ag_{13}, $Ag_{12}Cu_1$, $Cu_{12}Ag_1$, and pure Cu_{13} clusters with Ih, Dh, and COh simulated by the incident light of 514.5 nm at 10 K. All of the Raman spectra exhibit many significant vibrational modes. In Ag_{13} and $Ag_{12}Cu_1$ clusters with Ih (Fig. 5(a)), the intensity of the maximum peak of the $Ag_{12}Cu_{1core}$ cluster Raman spectrum is nearly twice as large as that of Ag_{13} and $Ag_{12}Cu_{1sur}$ clusters. For Ag_{13} and $Ag_{12}Cu_1$ clusters with Dh motif (Fig. 5(b)), the intensity of the maximum peak of the $Ag_{12}Cu_{1core}$ cluster Raman spectrum is nearly half of that of Ag_{13} and $Ag_{12}Cu_{1sur}$ clusters. For Ag_{13} and $Ag_{12}Cu_1$ clusters with COh motifs (Fig. 5(c)), the Raman spectrum of the $Ag_{12}Cu_{1core}$ cluster shows a new peak that obviously differs from that of Ag_{13} and $Ag_{12}Cu_{1sur}$ clusters. The new peak is located at 24.74 cm^{-1} and oscillator strength $f = 2.62$ a.u. The intensity of the maximum peak of $Ag_{12}Cu_{1core}$ intervenes with that of Ag_{13} and $Ag_{12}Cu_{1sur}$ clusters.

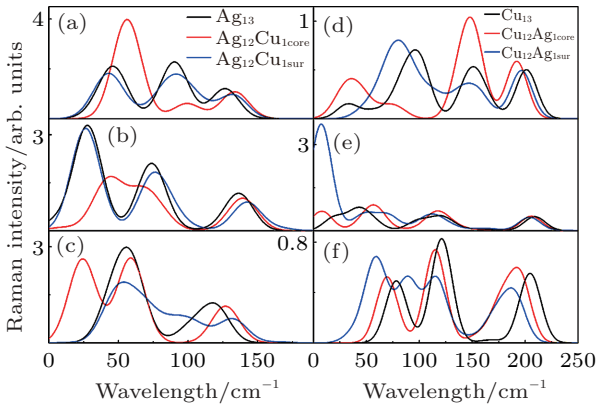


Fig. 5. (color online) Raman spectra for pure Ag_{13} and $Ag_{12}Cu_1$ (left) with Ih (a), Dh (b), and COh (c) motifs, and pure Cu_{13} and $Cu_{12}Ag_1$ (right) clusters with Ih (d), Dh (e), and COh (f) motifs calculated by GGA/DFT.

In Cu_{13} and $Cu_{12}Ag_1$ clusters with Ih (Fig. 5(d)), the Raman spectrum of the more stable $Cu_{12}Ag_{1sur}$ cluster does not

have a peak below wavelength 50 cm^{-1}. Moreover, the intensity of the maximum peak of the $Cu_{12}Ag_{1sur}$ cluster Raman spectrum intervenes with that of Cu_{13} and $Cu_{12}Ag_{1core}$ clusters. For Cu_{13} and $Cu_{12}Ag_1$ clusters with Dh motif (Fig. 5(e)), the intensity of the maximum peak of the $Cu_{12}Ag_{1sur}$ cluster Raman spectrum is quadplex as large as that of Cu_{13} and $Cu_{12}Ag_{1core}$ clusters. For Cu_{13} and $Cu_{12}Ag_1$ clusters with COh motif (Fig. 5(f)), the Raman spectrum of the $Cu_{12}Ag_{1sur}$ cluster shows a new small peak that is obviously absent in that of Cu_{13} and $Cu_{12}Ag_{1sur}$ clusters. The new peak is at 89.11 cm^{-1} and oscillator strength $f = 0.53$ a.u. The intensity of the maximum peak of the $Cu_{12}Ag_{1sur}$ cluster is smaller than that of Cu_{13} and $Cu_{12}Ag_{1core}$ clusters.

Figure 6 compares the vibrational spectra of pure Ag_{13}, $Ag_{12}Cu_1$, $Cu_{12}Ag_1$, and pure Cu_{13} clusters with Ih, Dh, and COh shapes simulated by GGA/DFT. All of the vibrational spectra exhibit many significant vibrational modes. The vibrations of the Ag_{13} cluster with Ih motif range within 60.11–183.11 cm^{-1} with the maximum oscillator strength f of 1.36 km/mol (171.11 cm^{-1}) (Fig. 6(a)), which is in agreement with the previous reports.[83,84] The vibrations of $Ag_{12}Cu_{1core}$ and $Ag_{12}Cu_{1sur}$ clusters with Ih motif range within 81.53–179.53 cm^{-1} and 61.16–196.16 cm^{-1}, respectively (Fig. 6(a)). The vibrations of Ag_{13}, $Ag_{12}Cu_{1core}$, and $Ag_{12}Cu_{1sur}$ clusters with Dh motif range within 61.97–159.97 cm^{-1}, 42.66–149.66 cm^{-1}, and 62.92–165.92 cm^{-1}, respectively (Fig. 6(b)). The vibrations of Ag_{13}, $Ag_{12}Cu_{1core}$, and $Ag_{12}Cu_{1sur}$ clusters with COh motif range within 22.84–159.84 cm^{-1}, 69.62–155.62 cm^{-1}, and 44.03–174.02 cm^{-1}, respectively (Fig. 6(c)).

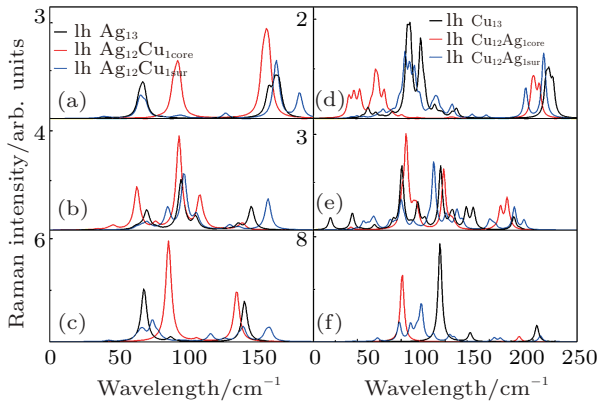


Fig. 6. (color online) Vibrational spectra for pure Ag_{13} and $Ag_{12}Cu_1$ (left) with Ih (a), Dh (b), and COh (c) motifs, and pure Cu_{13} and $Cu_{12}Ag_1$ (right) clusters with Ih (d), Dh (e), and COh (f) motifs calculated by GGA/DFT. The FWHM is 5 cm^{-1}.

The vibrations of Cu_{13}, $Cu_{12}Ag_{1core}$, and $Cu_{12}Ag_{1sur}$ clusters with Ih motif range within 58.91–280.91 cm^{-1}, 34.63–264.63 cm^{-1}, and 73.12–271.12 cm^{-1}, respectively (Fig. 6(d)). The vibrations of Cu_{13}, $Cu_{12}Ag_{1core}$, and $Cu_{12}Ag_{1sur}$ clusters with Dh motif range within 14.94–234.94 cm^{-1}, 42.38–229.38 cm^{-1}, and 52.72–264.72 cm^{-1}, respectively (Fig. 6(e)). The vibrations of Cu_{13}, $Cu_{12}Ag_{1core}$, and $Cu_{12}Ag_{1sur}$ clusters with COh motif range within 121.96–262.96 cm^{-1}, 82.49–238.49 cm^{-1}, and 68.35–263.35 cm^{-1}, respectively (Fig. 6(f)).

The ranges of the vibrational spectra of Ag_{13} and $Ag_{12}Cu_1$ clusters are smaller than those of Cu_{13} and $Cu_{12}Ag_1$ clusters. The ranges of the vibrational spectra of Ag_{13} and $Ag_{12}Cu_1$ or Cu_{13} and $Cu_{12}Ag_1$ clusters with Ih motif are wider than those with Dh and COh, and the ranges of the vibrational spectra of Ag_{13} and $Ag_{12}Cu_1$ or Cu_{13} and $Cu_{12}Ag_1$ clusters with Dh motifs are larger than those with COh. However, the intensities of the vibrational spectra of Ag_{13} and $Ag_{12}Cu_1$ or Cu_{13} and $Cu_{12}Ag_1$ clusters increase as the shape of the clusters changes from Ih to Dh and to COh. These vibrational spectra indicate that the maximum oscillator strength is related to the cluster structure.

In summary, our calculations demonstrate that the stabilities of the Ag_{13}, $Ag_{12}Cu_1$, Cu_{13}, and $Cu_{12}Ag_1$ clusters with different motifs (Ih, Dh, or COh) are determined by the strain relaxation, the bond strengths, the bond lengths, the bond number, the surface energies, and the charge transfer. Our results also indicate that the surface plasmon polariton behaviors of pure silver, pure copper, and single atom-doped Ag–Cu nanoalloys open the possibility of new applications for 13-atom Ag–Cu nanoalloys in nonlinear optical films and devices. The vibrational and Raman spectroscopy may be helpful in determining the cluster size and structure.

4. Conclusions

We investigate the stabilities and optical, Raman, and vibrational properties of Ag_{13}, $Ag_{12}Cu_1$, Cu_{13}, and $Cu_{12}Ag_1$ clusters with different motifs (Ih, Dh, or COh) by GGA/PBE/DFT. The results show that the most stable structures of the clusters are COh for Ag_{13}, Ih for Cu_{13}, Ih for $Ag_{12}Cu_{1core}$, and Ih for $Cu_{12}Ag_{1sur}$. The strain relaxation, the bond number, the surface energy, and the charge transfer determine the stabilities of $Ag_{12}Cu_1$ and $Cu_{12}Ag_1$ clusters. The position energies of the UV–Vis optical absorption of pure Ag_{13} clusters are in excellent agreement with the experiment results. In the Vis–NIR optical absorption, the results show the following red shifts: 1) clusters change from $Ag_{12}Cu_{1core}$ to Ag_{13} to $Ag_{12}Cu_{1sur}$ with the same motifs, 2) the shapes of pure Ag_{13} and $Ag_{12}Cu_{1core}$ clusters change from COh to Ih to Dh, 3) the shape of $Ag_{12}Cu_{1sur}$ clusters changes from Ih to COh to Dh, and 4) the shapes of pure Cu_{13} and $Cu_{12}Ag_1$ clusters change from Ih to Dh to COh. All of the Raman and vibrational spectra exhibit many significant vibrational modes. The intensities of the maximum peaks of the Ag_{13} and $Ag_{12}Cu_1$ cluster Raman spectra are much stronger than those of $Cu_{12}Ag_1$ and pure Cu_{13} clusters (except the Dh $Cu_{12}Ag_{1sur}$ cluster). The ranges of the vibrational spectra of Ag_{13} and $Ag_{12}Cu_1$ clusters are

smaller than those of Cu_{13} and $Cu_{12}Ag_1$ clusters. The ranges of the vibrational spectra of Ag_{13} and $Ag_{12}Cu_1$ or Cu_{13} and $Cu_{12}Ag_1$ clusters with Ih motifs are wider than those with Dh and COh motifs, and the ranges of the vibrational spectra of Ag_{13} and $Ag_{12}Cu_1$ or Cu_{13} and $Cu_{12}Ag_1$ clusters with Dh motif are wider than those with COh.

References

[1] Zhu M, Aikens C M, Hollander F J, Schatz G C and Jin R 2008 *J. Am. Chem. Soc.* **130** 5883
[2] Aikens C M 2008 *J. Phys. Chem. C* **112** 19797
[3] Huang T and Murray R W 2001 *J. Phys. Chem. B* **105** 12498
[4] Link S, Beeby A, FitzGerald S, El-Sayed M A, Schaaff T G and Whetten R L 2002 *J. Phys. Chem. B* **106** 3410
[5] Ramakrishna G, Varnavski O, Kim J, Lee D and Goodson T 2008 *J. Am. Chem. Soc.* **130** 5032
[6] Zhu M Z, Aikens C M, Hendrich M P, Gupta R, Qian H F, Schatz G C and Jin R C 2009 *J. Am. Chem. Soc.* **131** 2490
[7] Chen Y S, Choi H and Kamat P V 2013 *J. Am. Chem. Soc.* **135** 8822
[8] Sakai N, Nakamura S and Tatsuma T 2013 *Dalton T.* **42** 16162
[9] Darbha G K, Ray A and Ray P C 2007 *ACS Nano* **1** 208
[10] Mirkin C A, Letsinger R L, Mucic R C and Storhoff J J 1996 *Nature* **382** 607
[11] Brongersma M L, Hartman J W and Atwater H A 2000 *Phys. Rev. B* **62** 16356
[12] Quinten M, Leitner A, Krenn J R and Aussenegg F R 1998 *Opt. Lett.* **23** 1331
[13] Lewis L N 1993 *Chem. Rev.* **93** 2693
[14] Ferrando R, Jellinek J and Johnston R L 2008 *Chem. Rev.* **108** 845
[15] Jellinek J 2008 *Faraday Discuss* **138** 11
[16] Zhang J T, Li J and Sheng Y 2014 *Chin. Phys. B* **23** 013103
[17] Meng X X, Fan J, Bao K, Li F F, Huang X L, Li Y, Tian F B, Duan D F, Jin X L, Zhu P W, He Z, Zhou Q, Gao C X, Liu B B and Cui T 2014 *Chin. Phys. B* **23** 016102
[18] Zheng X H, Sui J H, Zhang X, Yang Z Y and Cai W 2014 *Chin. Phys. B* **23** 018101
[19] Zhang S, Qin Y, Ma M F, Lu C and Li G Q 2014 *Chin. Phys. B* **23** 013601
[20] Scholl J A, Koh A L and Dionne J A 2012 *Nature* **483** 421
[21] Lee K S and El-Sayed M A 2006 *J. Phys. Chem. B* **110** 19220
[22] Noguez C 2007 *J. Phys. Chem. C* **111** 3806
[23] Dong J Z, Zhang X L, Cao Y A, Yang W S and Tian J G 2011 *Mater. Lett.* **65** 2665
[24] Gong J X, Zhou F, Li Z Y and Tang Z Y 2012 *Langmuir* **28** 8959
[25] Guidez E B, Makinen V, Hakkinen H and Aikens C M 2012 *J. Phys. Chem. C* **116** 20617
[26] Baishya K, Idrobo J C, Ogut S, Yang M L, Jackson K and Jellinek J 2008 *Phys. Rev. B* **78** 075439
[27] Durante N, Fortunelli A, Broyer M and Stener M 2011 *J. Phys. Chem. C* **115** 6277
[28] Weissker H C and Mottet C 2011 *Phys. Rev. B* **84** 165443
[29] Bae G T and Aikens C M 2012 *J. Phys. Chem. C* **116** 10356
[30] Ma W Q and Chen F Y 2012 *J. Alloy. Compd.* **541** 79
[31] Li W Y and Chen F Y 2013 *J. Nanopart. Res.* **15** 1809
[32] Rao Y, Lei Y M, Cui X Y, Liu Z W and Chen F Y 2013 *J. Alloy. Compd.* **565** 50
[33] Li W and Chen F 2014 *Comp. Mater. Sci.* **81** 587
[34] Li W and Chen F 2014 *Eur. Phys. J. D* **68** 91
[35] Li W and Chen F 2014 *Phys. B* **443** 6
[36] Li W and Chen F 2014 *J. Alloy. Compd.* **607** 238
[37] Li W and Chen F 2013 *Appl. Phys. A Mater.* **113** 543
[38] Binns C 2001 *Surf. Sci. Rep.* **44** 1
[39] Knickelbein M B 1999 *Ann. Rev. Phys. Chem.* **50** 79
[40] Tsuji M, Tang X L, Matsunaga M, Maeda Y and Watanabe M 2010 *Cryst. Growth Des.* **10** 5238
[41] Tsuji M, Ogino M, Matsuo R, Kumagae H, Hikino S, Kim T and Yoon S H 2010 *Cryst. Growth Des.* **10** 296
[42] Zeng J, Zheng Y Q, Rycenga M, Tao J, Li Z Y, Zhang Q A, Zhu Y M and Xia Y N 2010 *J. Am. Chem. Soc.* **132** 8552
[43] Chen F Y and Johnston R L 2007 *Appl. Phys. Lett.* **90** 153123
[44] Harb M, Rabilloud F, Simon D, Rydlo A, Lecoultre S, Conus F, Rodrigues V and Felix C 2008 *J. Chem. Phys.* **129** 194108
[45] Idrobo J C, Ogut S, Nemeth K, Jellinek J and Ferrando R 2007 *Phys. Rev. B* **75** 233411
[46] Oviedo J and Palmer R E 2002 *J. Chem. Phys.* **117** 9548
[47] Longo R C and Gallego L J 2006 *Phys. Rev. B* **74** 193409
[48] Chang C M and Chou M Y 2004 *Phys. Rev. Lett.* **93** 133401
[49] Yang M, Jackson K A and Jellinek J 2006 *J. Chem. Phys.* **125** 144308
[50] Yang M L, Jackson K A, Koehler C, Frauenheim T and Jellinek J 2006 *J. Chem. Phys.* **124** 024308
[51] Zeng Q, Wang X, Yang M L and Fu H B 2010 *Eur. Phys. J. D* **58** 125
[52] Baishya K, Idrobo J C, Ogut S, Yang M L, Jackson K A and Jellinek J 2011 *Phys. Rev. B* **83** 245402
[53] Delley B 1990 *J. Chem. Phys.* **92** 508
[54] Delley B 2000 *J. Chem. Phys.* **113** 7756
[55] Delley B 2002 *Phys. Rev. B* **66** 155125
[56] Perdew J P, Burke K and Ernzerhof M 1996 *Phys. Rev. Lett.* **77** 3865
[57] Chen F and Johnston R L 2008 *Acta Mater.* **56** 2374
[58] Delley B 2010 *J. Phys.: Condens. Matter* **22** 384208
[59] Bechthold P S, Kettler U and Krasser W 1985 *Surf. Sci.* **156** 875
[60] Fedrigo S, Harbich W and Buttet J 1993 *Phys. Rev. B* **47** 10706
[61] Idrobo J C, Ogut S and Jellinek J 2005 *Phys. Rev. B* **72** 085445
[62] Ogut S, Idrobo J C, Jellinek J and Wang J L 2006 *J. Clust. Sci.* **17** 609
[63] Tiago M L, Idrobo J C, Ogut S, Jellinek J and Chelikowsky J R 2009 *Phys. Rev. B* **79** 155419
[64] Yabana K and Bertsch G F 1999 *Phys. Rev. A* **60** 3809
[65] Yan J and Gao S W 2008 *Phys. Rev. B* **78** 235413
[66] Shin K, Kim D H, Yeo S C and Lee H M 2012 *Catal. Today* **185** 94
[67] Chang C M and Chou M Y 2004 *Phys. Rev. Lett.* **93** 133401
[68] Longo R C and Gallego L J 2006 *Phys. Rev. B* **74** 193409
[69] Michaelian K, Rendon N and Garzon I L 1999 *Phys. Rev. B* **60** 2000
[70] Oviedo J and Palmer R E 2002 *J. Chem. Phys.* **117** 9548
[71] Pereiro M, Baldomir D and Arias J E 2007 *Phys. Rev. A* **75** 063204
[72] Yang M, Jackson K A and Jellinek J 2006 *J. Chem. Phys.* **125** 144308
[73] Yang M L, Jackson K A, Koehler C, Frauenheim T and Jellinek J 2006 *J. Chem. Phys.* **124** 024308
[74] Yang X L, Cai W S and Shao X G 2007 *J. Phys. Chem. A* **111** 5048
[75] Baishya K, Idrobo J C, Ogut S, Yang M L, Jackson K A and Jellinek J 2011 *Phys. Rev. B* **83** 245402
[76] Darby S, Mortimer-Jones T V, Johnston R L and Roberts C 2002 *J. Chem. Phys.* **116** 1536
[77] Zeng Q, Wang X, Yang M L and Fu H B 2010 *Eur. Phys. J. D* **58** 125
[78] Bochicchio D and Ferrando R 2010 *Nano Lett.* **10** 4211
[79] Ferrando R, Jellinek J and Johnston R L 2008 *Chem. Rev.* **108** 845
[80] Mottet C, Rossi G, Baletto F and Ferrando R 2005 *Phys. Rev. Lett.* **95** 035501
[81] Bochicchio D and Ferrando R 2013 *Phys. Rev. B* **87** 165435
[82] Idrobo J C and Pantelides S T 2010 *Phys. Rev. B* **82** 085420
[83] Ozin G A and Mcintosh D F 1986 *J. Phys. Chem.* **90** 5756
[84] Yang F and Liu L 1995 *J. China Univ. Sci. Tech.* **25** 512